SOI Induced Exchange Anisotropy in Germanium Bilayers

by

Erik Lemmens Sjöstrand

To obtain the degree of Bachelor of Science
at the Delft University of Technology.
To be defended publicly on Friday July 12, 2024 at 10:00.

Student number:	5533635	
Thesis committee:	Prof. dr. ir. M. Veldhorst,	QuTech, (Responsible supervisor)
	Prof. dr. A. Chatterjee,	QuTech, TU Delft
Supervisor:	dr. ir. S. Bosco,	QuTech, TU Delft

Abstract

Germanium heterostructures are frontrunners for semiconducting quantum information processing. State-of-the-art double quantum dots are confined in monolayers of Germanium, however recent technological advances enable double quantum dots to be confined vertically in germanium bilayers, offering the opportunity add the vertical degree of freedom to the qubit architecture. This project consists in theoretically modelling the double quantum dot in a Germanium bilayer by finding an effective Hamiltonian of two interacting spins in the presence of spin-orbit interactions. By analyzing the anisotropy of the Landé g-factors in the double quantum dot, the project aims to identify opportunities and challenges for two-qubit gates implemented in these structures.

Contents

- Chapter 1 -

Introduction

Several requirements for quantum computation have been listed since the birth of the quantum computer concept in the late 20^{th} century, such as the need for storage in a scalable quantum register (quantum bits), the requirement for possible preparation in a fiducial state, as well as need of sufficient coherence, attainability of a set of high-fidelity gates and finally the ability of reading out the register at the end of a computation [1]. Using the spin degree of freedom of an electron confined in a potential has proven to be an appropriate choice for a computational unit, as the particle's spin-up and spin-down state naturally define the qubit. Furthermore, using electron spins allows electric initialization and high-fidelity read-out employing tunneling or the Pauli exclusion principle [2].
Semiconductor spin qubits share the characteristics of the spin being confined to isolated sites. By engineering the density of conducting electrons, the electron motion can be restricted to two dimensions and allows for the localization of the particles in quantum dots (QDs) providing an appropriate setting for spin-based quantum information processing [3].
Across distinguishable locations, the wavefunctions of two electrons can overlap and decrease the energy of the spin-singlet state relative to the symmetric spin-triplet states. This energy decrease is commonly referred to as the exchange coupling J and is especially relevant, from a quantum control point of view, due to its tunability over large energy intervals through adjustment of the gate voltage [4].
The final goal of these QD arrangements is to work as quantum gates, where notable 2-qubit gates that arise from this specific setup are the so-called $SWAP$-gate and $\sqrt{SWAP}$-gate [4].

In recent years, Germanium has proven itself to be a good candidate as a heterostructure material for quantum computation purposes [5]. It is a group IV semiconductor with several interesting and useful properties, such as its ability to form high-quality quantum wells and QDs and its strong spin-orbit coupling which allows for precise electrical control of spin states in the QDs.
Until now, the most studied form of QDs in Germanium has consisted of observing double quantum dots (DQDs) confined in monolayer structures. Recent technological advances in the field, however, have enabled vertical confinement of DQDs in Germanium bilayers, allowing the addition of the vertical degree of freedom to the qubit architecture.

This thesis project aims to theoretically model the DQD in a Germanium bilayer by finding an effective Hamiltonian of two interacting spins in the presence of spin-orbit interactions.
In Chap. 2 the theoretical model used for the project is discussed, starting from the general descriptions of single and double quantum dots and their respective Hamiltonians. This chapter also treats the Schrieffer-Wolff transformation, a crucial tool that allows us to project large Hamiltonians onto a smaller subspace, providing a basis where the effective exchange coupling can be identified and expressed using the parameters of the QD. Finally, the chapter introduces the Luttinger-Kohn Hamiltonian, which describes the behavior of charge carriers and provides the framework for band structure and spin-orbit interaction analysis in group IV semiconductors such as Germanium. Additionally, the dimensional reduction of the 3D Luttinger-Kohn Hamiltonian to a simpler 2D version is explained and justified. In section 3 the Germanium bilayer model is analyzed. We observe how the energy levels of the Luttinger-Kohn Hamiltonian are discretized and how we use the Schrieffer-Wolff transformation to obtain an effective low-energy Hamiltonian without neglecting higher-energy contributions.
Finally, section 4 gives a conclusion and outlook for further theoretical research that can be done within the field.

- Chapter 2 -

Theoretical Model

2.1. Single Quantum Dot (SQD)

2.1.1. Designing the quantum dot

An electron can be confined to two dimensions due to the layer structure of the semiconductor in which it resides, specifically in a narrow quantum well in the case of a Germanium semiconductor. This type of two-dimensional conducting layer is known as a 2D electron gas, or 2DEG. Through the use of gate electrodes on the surface of the material, the 2DEG is locally depleted around the desired quantum dot to create a potential well in which the electron spin can be confined. The gates are also used to increase the resistance between the dot and the adjacent electron gas, allowing for localization of the spin in the dot [6]. Completely removing all electrons from a quantum dot is difficult, because it requires large voltages on the gate electrodes which leads to challenges making electrons enter and leave the dot. For this reason, careful design of gate electrodes is needed in a way that differentiates 'plunger' gates, which control the number of electrons in the dot, from 'lead' gates, which control the coupling to the adjacent 2DEG.
To prevent any thermal excitation of the electron and ensure that the spin qubit can be operated in its lowest available energy states, the system needs to be brought down to very low temperatures, typically in the order of 10mK to 4K [7][8].

2.1.2. Loss-DiVincenzo qubit

The simplest quantum bit is the so-called Loss-DiVincenzo qubit [6]. It consists of a single electron confined in a quantum dot where information is encoded using the electron's intrinsic spin-$\frac{1}{2}$ state. The logical subspace considered for this system consists of the states $|\uparrow\rangle$ and $|\downarrow\rangle$, for which the energy degeneracy can be lifted using a static magnetic field resulting in Zeeman splitting. Applying an oscillating field in the direction perpendicular to the static field allows to drive oscillations of the spin around the Bloch sphere, and thus enables control of the qubit. The Hamiltonian of the single spin in a SQD can be expressed as

$$H = g\mu_B \mathbf{B}\cdot\hat{\mathbf{S}} = g\mu_B(B_z\sigma_z + B_x\sigma_x\cos(\omega t+\phi)) \tag{2.1}$$

where g is the material-dependent Landé g-factor, μ_B is the Bohr magneton and ω and ϕ are the frequency and the phase of the oscillating field, and where we have assumed that the static and oscillating magnetic fields are applied in the z- and x-direction respectively. For the resonant case, $\omega = g\mu_B B_z/\hbar$.

2.1.3. Spin-orbit interaction

An electron moving in proximity of a charged particle with velocity $\mathbf{v}$, such as the case of an electron passing through a crystal lattice, will feel the local electric field $\mathbf{E}$ caused by the nucleus, and will therefore experience a magnetic field $\mathbf{B}_{\text{eff}}$. This induces an interaction with the spin of the electron through the Zeeman energy resulting in so-called spin-orbit interaction (SOI). It can be described by a Hamiltonian of the following form:

$$H_{\text{SOI}} = a\mathbf{E}\cdot(\mathbf{p}\times\boldsymbol{\sigma}) \tag{2.2}$$

where a is a constant depending on the type of SOI, and where one can clearly see that the spin $\boldsymbol{\sigma}$ and the momentum $\mathbf{p}$ are related [9]. In some materials, with Germanium being a prime example, the SOI is so strong that spin and momentum can no longer be separated [10]. This interaction allows for another type of qubit driving mechanism called Electric-Dipole Spin Resonance (EDSR). The technique is based on shifting the position of the quantum dot by applying an AC electric field in the direction of the nanowire or in the plane of the semiconducting layer. This enables fully electrical qubit control without any need for magnetic fields, which presents advantages in integration into semiconductor technology as well as facilitated control and localization [10]. Finally, spin-orbit interaction gives rise to anisotropy in the particle exchange energy, which will become important later when we consider the exchange in double quantum dots in Germanium bilayers.

2.2. Double Quantum Dot (DQD)

Double quantum dots are often used instead of single quantum dots because they offer more sophisticated control and additional functionalities that are valuable for more advanced applications in quantum computing and quantum information processing.
Introducing a second electron into the dot system allows for coupling between the spins in the two dots, which can precisely be tuned and implemented for two-qubit gate operations. Furthermore, DQDs have an edge over SQDs when it comes to both the creation of entangled states between electrons of different dots and mitigation of decoherence.

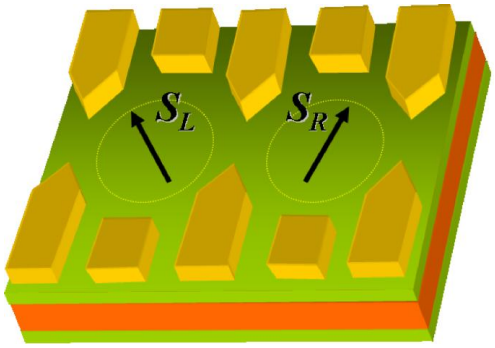

Figure 2.1: A double quantum dot. Similarly to the SQD, electrons are confined to a 2DEG in the circular regions shown. By applying a negative voltage to the back gate, the dots are depleted of electrons such that only one spin remains in each dot. The left (right) electron is represented by an arrow with a corresponding spin-1/2 operator $\hat{S}_{L(R)}$. The up and down eigenstates of the electrons encode the qubit [11].

The addition of the second electron, however, adds a number of different interactions and phenomena which need to be accounted for in the Hamiltonian of the DQD. In the following subsections we will address these interactions and formulate an effective Hamiltonian for the system.

2.2.1. Singlet-triplet basis

The two electrons in a double quantum dot are fermions, meaning they obey the Pauli exclusion principle. This principle states that two or more electrons in a quantum system cannot simultaneously occupy the same quantum state, and results in the requirement of the total wavefunction of the two electrons in the system to be odd under the exchange of all degrees of freedom.
We expect the electrons to be localized in each dot, which leaves us with a convenient spin basis to work with for our description of the system. We are left with an anti-symmetric spin-singlet state:

$$|S\rangle = \frac{|\uparrow\downarrow\rangle - |\downarrow\uparrow\rangle}{\sqrt{2}}$$

and three symmetric spin-triplet states:

$$|T_+\rangle = |\uparrow\uparrow\rangle$$
$$|T_0\rangle = \frac{|\uparrow\downarrow\rangle + |\downarrow\uparrow\rangle}{\sqrt{2}}$$
$$|T_-\rangle = |\downarrow\downarrow\rangle$$

Note that there are two additional spin-singlet states $|S_L\rangle$ and $|S_R\rangle$ that are associated with symmetric orbital wavefunctions corresponding to when the electrons are confined in the same dot, either left or right. These states will become important later when finding the effective Hamiltonian.

2.2.2. Orbital Hamiltonian

Before considering the interactions between the two electrons in the double quantum dot, it is important to establish the energies related to the single electrons, more specifically their orbital localization, in the DQD system. We define $|L\rangle$ and $|R\rangle$ to be the ground states of the left and the right dot, with corresponding eigenenergies ϵ_L and ϵ_R. When the dots are far apart, the electron can be either in the left or in the right

dot, which helps us formulate an associated Hamiltonian based on the difference $\epsilon = \epsilon_L - \epsilon_R$ between the eigenenergies of the left and right dot as shown in figure 2.2.

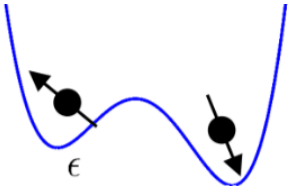

Figure 2.2: The detuning Hamiltonian is determined by the difference in energy level between the left and the right dot, ϵ. The tunneling Hamiltonian is determined by the likelihood of the electron hopping from one dot to another, t.

The energy difference is commonly known as detuning, and results in the Hamiltonian H_{detuning}:

$$H_{\text{detuning}} = \epsilon_L |L\rangle\langle L| + \epsilon_R |R\rangle\langle R| = \frac{\epsilon}{2}[|L\rangle\langle L| - |R\rangle\langle R|]\left(+\frac{\epsilon_l + \epsilon_R}{2}[|L\rangle\langle L| + |R\rangle\langle R|]\right) = \frac{\epsilon}{2}\tau_z \tag{2.3}$$

where the part in brackets is omitted since it causes a global shift in energy without influencing the dynamics of the system.
There is also energy associated with tunneling t of the particle between the dots as they are pushed closer together, which is contained in the Hamiltonian $H_{\text{tunneling}}$:

$$H_{\text{tunneling}} = -t[|L\rangle\langle R| + |R\rangle\langle L|] = -t\tau_x \tag{2.4}$$

Finally, we add these two contributions to get the single-electron orbital Hamiltonian, which is applied to both electrons in a two-electron DQD system:

$$H_{\text{orbital}} = (\frac{\epsilon}{2}\tau_z^{(1)} - t\tau_x^{(1)}) + (\frac{\epsilon}{2}\tau_z^{(2)} - t\tau_x^{(2)}) \tag{2.5}$$

where τ_z and τ_x denote two Pauli-like matrices acting on the dot positions and where the superscripts 1 and 2 denote the first and the second electron respectively. Using the basis of the spin-singlet and triplet states mentioned in the previous subsection, a Hamiltonian matrix can be constructed. It turns out however, that the absence of spin dependence in this Hamiltonian causes a decoupling of the singlet and triplet sectors, and in fact produces only zero terms in the triplet sector due to the anti-symmetry of the triplet orbital states.

2.2.3. Zeeman field, Coulomb interaction and exchange J

Similar to the SQD, we want to apply a magnetic field to the double dot system which will couple to the spins through the Zeeman Hamiltonian. Because the field couples to both electrons, we need to apply equation 2.1 to the individual spins as such:

$$H_{\text{Zeeman}} = H_{\text{Zeeman}}^{(1)} + H_{\text{Zeeman}}^{(2)} = \frac{g\mu_B}{2}\mathbf{B}\cdot(\boldsymbol{\sigma}^{(1)} + \boldsymbol{\sigma}^{(2)}) \tag{2.6}$$

Unlike H_{orbital}, H_{Zeeman} is only dependent on spin. This also results in decoupling of the singlet and the triplet sector, and the anti-symmetry of the singlet spin states gives an all-zero singlet sector.
Two electrons in proximity will try to repel each other due to Coulomb interaction. Also this interaction needs to be taken into account in the full Hamiltonian. Because Coulomb repulsion is spin-independent, no coupling of the singlet and triplet sector will take place, and will only affect the singlet sector (the triplet sector only undergoes a global energy shift which can be omitted). The Coulomb potential is formulated as follows:

$$V_{\text{Coulomb}}(\mathbf{r_1}, \mathbf{r_2}) = \frac{e^2}{4\pi\varepsilon|\mathbf{r_1} - \mathbf{r_2}|} \tag{2.7}$$

where e is the electron charge and ε is the permittivity of the material.
Using the Hamiltonian terms expressed so far, a full Hamiltonian can be constructed in the singlet-triplet basis using $\langle\psi_i| H_{\text{DQD}} |\psi_j\rangle$, where $H_{\text{DQD}} = H_{\text{orbital}} + H_{\text{Zeeman}} + V_{\text{Coulomb}}$, resulting in the following matrix:

$$H_{\text{DQD}} = \begin{bmatrix} U+\epsilon & 0 & -\sqrt{2}t & 0 & 0 & 0 \\ 0 & U-\epsilon & -\sqrt{2}t & 0 & 0 & 0 \\ -\sqrt{2}t & -\sqrt{2}t & 0 & 0 & 0 & 0 \\ 0 & 0 & 0 & g\mu_B B_z & 0 & 0 \\ 0 & 0 & 0 & 0 & -g\mu_B B_z & 0 \\ 0 & 0 & 0 & 0 & 0 & 0 \end{bmatrix} \tag{2.8}$$

where U represents the Coulomb repulsion between electrons confined in the same dot and where we for simplicity have rotated the system such that the magnetic field is applied in the z-direction. It should be noted that all other terms in the singlet sector related to Coulomb interaction have been dropped due to their small contribution in comparison to U, an approximation associated with the Hubbard model which is justified by the weak tunnel coupling [12].
Ultimately, we are most interested in the case where the electron spins are confined in different dots. In other words, we only want to consider the low-energy subspace of the Hamiltonian corresponding to the $|S_0\rangle$ state and the three triplet states. By assuming the absence of a magnetic field treating the tunneling terms in H_{DQD} as a perturbation, we use standard perturbation theory to find that the energy of $|S_0\rangle$ is lowered by a certain amount, the exchange energy J, making the singlet state the ground state at zero magnetic:

$$J = \frac{2t^2}{U+\epsilon} + \frac{2t^2}{U-\epsilon} \tag{2.9}$$

The exchange coupling arises from the overlap of the wavefunction of the two spins and the Pauli exclusion principle, and is often included in simple models in the form of the Heisenberg (isotropic) exchange Hamiltonian:

$$H_{\mathrm{ex}} = \frac{J}{4}\boldsymbol{\sigma}^{(1)} \cdot \boldsymbol{\sigma}^{(2)} \tag{2.10}$$

J is especially important for quantum computation because it is a parameter that is easily tunable and controlled. This makes it the foundation of the basic two-qubit quantum gate, allowing for operations such as controlled-NOT and SWAP.

2.2.4. Spin-orbit interaction in DQDs

So far, the different components of the DQD Hamiltonian have not resulted in any mixing of the singlet and triplet states. Furthermore, the system doesn't exhibit any anisotropy concerning the exchange coupling. The spins in a double dot, analogously to the single dot, experience spin-orbit interaction which, unlike the aforementioned interactions, couple the singlet and triplet sectors. In the DQD, spin-orbit interaction causes differing Landé g-factors in the two dots due to e.g. different dot sizes, as well as spin non-conserving tunnel coupling between the dots. For a single electron, the Hamiltonian can now be written as:

$$H = \frac{\epsilon}{2}\tau_z - t_0\tau_x + \frac{g\mu_B B_z}{2}\sigma_z + \frac{\delta_z g\mu_B B_z}{2}\tau_z\sigma_z + \frac{\delta g_x\mu_B B_z}{2}\tau_z\sigma_x + \frac{\delta g_y\mu_B B_z}{2}\tau_z\sigma_y - t_{SO}\tau_y\sigma_y \tag{2.11}$$

where t_0 is the spin-conserving tunnel coupling, t_{SO} is the spin-flip (non-conserving) tunnel coupling and δg is the difference in g-factor. Using the same method as in the previous subsection, we obtain a Hamiltonian matrix for the DQD:

$$H_{\mathrm{DQD}} = \begin{bmatrix} U+\epsilon & 0 & -\sqrt{2}t_0 & -t_{\mathrm{SO}} & -t_{\mathrm{SO}} & 0 \\ 0 & U-\epsilon & -\sqrt{2}t_0 & -t_{\mathrm{SO}} & -t_{\mathrm{SO}} & 0 \\ -\sqrt{2}t_0 & -\sqrt{2}t_0 & 0 & -\frac{\delta b_x+i\delta b_y}{\sqrt{2}} & \frac{\delta b_x-i\delta b_y}{\sqrt{2}} & \delta g\mu_B B_z \\ -t_{\mathrm{SO}} & -t_{\mathrm{SO}} & -\frac{\delta b_x-i\delta b_y}{\sqrt{2}} & g\mu_B B_z & 0 & \frac{b_x-ib_y}{\sqrt{2}} \\ -t_{\mathrm{SO}} & -t_{\mathrm{SO}} & \frac{\delta b_x+i\delta b_y}{\sqrt{2}} & 0 & -g\mu_B B_z & \frac{b_x+ib_y}{\sqrt{2}} \\ 0 & 0 & \delta g\mu_B B_z & \frac{b_x+ib_y}{\sqrt{2}} & \frac{b_x-ib_y}{\sqrt{2}} & 0 \end{bmatrix} \tag{2.12}$$

where $\delta b = \mu\mathbf{B}\cdot(\hat{g}_1 - \hat{g}_2)/2$ is the gradient Zeeman field due to differing g-factors between the dots. Due to the coupling of orbital and spin degrees of freedom in the newly added terms, the singlet and triplet sectors are mixed. What this ultimately results in is the introduction of anisotropy in the exchange coupling. To find the exchange, one can utilize the spin rest frame to eliminate the spin-flip tunneling and regard the SOI as only affecting the g-factors of the dots, causing the spin to experience a gradient Zeeman field. The frame change is performed through a unitary transformation where the spin and orbital degrees of freedom are mixed by the local spin-flip rotation. Putting it in the singlet-triplet basis of single occupied dots yields the following 4×4 Hamiltonian:

$$\begin{bmatrix} -J & -\frac{\delta b_x+i\delta b_y}{\sqrt{2}} & \frac{\delta b_x-i\delta b_y}{\sqrt{2}} & \delta b_z \\ -\frac{\delta b_x-i\delta b_y}{\sqrt{2}} & b_z & 0 & \frac{b_x-ib_y}{\sqrt{2}} \\ \frac{\delta b_x+i\delta b_y}{\sqrt{2}} & 0 & -b_z & \frac{b_x+ib_y}{\sqrt{2}} \\ \delta b_z & \frac{b_x+ib_y}{\sqrt{2}} & \frac{b_x-ib_y}{\sqrt{2}} & 0 \end{bmatrix} \tag{2.13}$$

where $b = \mu \mathbf{B} \cdot (\hat{g}_1 + \hat{g}_2)/2$ is the average Zeeman field from differing g-factors. In this frame, the exchange is isotropic, but to represent the exchange in our original lab frame, a rotation must be incorporated into the exchange. This results in a form different from Eq.2.10; we now have to consider the exchange as a matrix $\mathscr{J}$ acting on the spins[13]:

$$H_{\text{anisotropic}} = \frac{1}{4} \boldsymbol{\sigma_1} \cdot \mathscr{J} \boldsymbol{\sigma_2} \tag{2.14}$$

The exchange matrix $\mathscr{J}$ is given by:

$$\mathscr{J} = J_0 R_{SO}\Big(-\frac{2d}{\lambda_{SO}}\Big) = J_0 R_{SO}(\varphi) \tag{2.15}$$

where d is the inter-dot distance, $\lambda_{SO} = \hbar / m\alpha E$ is the characteristic spin-orbit length and $R_{SO}(\varphi)$ is a counterclockwise rotation matrix around the direction of the spin-orbit field [13].
The anisotropy of the exchange can however also arise solely from differing g-factors, i.e. even without any SOI present. The angle is then found by diagonalizing the Zeeman fields of the two qubits individually and combining them into the exchange matrix $\mathscr{J}$. This results in a final angle rotation of the form:

$$\vartheta = \arctan\Big(\frac{\delta g_x}{g_0 - \delta g_z}\Big) - \arctan\Big(\frac{\delta g_x}{g_0 + \delta g_z}\Big) \tag{2.16}$$

for a system with no g-factor anisotropy in the y-direction, as is the case in the system we will consider in Chap.3.

2.3. Schrieffer-Wolff Transformation

In several instances in the derivations so far, the aim has been to obtain an effective Hamiltonian from a more complicated Hamiltonian that fully describes the quantum system, with the goal of determining characteristics that allow for control of a qubit gate. The Schrieffer-Wolff transformation is a mathematical degenerate perturbative technique used in quantum mechanics to perform this simplification and is particularly useful in dealing with systems where clear separation between energy scales is present, such as when certain coupling terms or interactions in the full Hamiltonian are much weaker than others (as is the case in germanium double dots). In many quantum systems, the full Hamiltonian H can be split into a dominating part H_0 and a small perturbation ηV:

$$H = H_0 + \eta V \tag{2.17}$$

where H_0 is the unperturbed Hamiltonian. The Schrieffer-Wolff transformation is then constructed such that interactions between weakly interacting subspaces are decoupled and vanish, resulting in an effective Hamiltonian that only acts within a desired low-energy subspace. This section is largely based on the work of Sergey Bravyi, David P. DiVincenzo and Daniel Loss [14], where more details and proofs can be found.

We let $\mathscr{P}_0$ and $\mathscr{P}$ be a pair of linear subspaces of the same dimension of a finite-dimensional Hilbert space $\mathscr{H}$, with corresponding projectors P_0 and P. $\mathscr{P}_0$ is spanned by all eigenvectors of the unperturbed Hamiltonian H_0 with eigenvalues lying within a certain interval $\mathscr{J}_0 \subseteq \mathbb{R}$. Similarly, $\mathscr{P}$ is spanned by eigenvectors of a perturbed Hamiltonian $H = H_0 + \eta V$ with eigenvalues within an interval $\mathscr{J} \subseteq \mathbb{R}$ obtained by extending $\mathscr{J}_0$. We want to find a unitary transformation $U = e^S$, where S is an anti-Hermitian matrix ($S = -S^\dagger$), which gives a direct rotation from the subspace $\mathscr{P}$ to the low-energy subspace $\mathscr{P}_0$. This is the Schrieffer-Wolff transformation [14]. We then find the effective low-energy Hamiltonian H_{eff}:

$$H_{\text{eff}} = P_0 U (H_0 + \eta V) U^\dagger P_0 \tag{2.18}$$

However, due to a lack of knowledge about $\mathscr{P}$ in most applications of the theory, equation 2.18 cannot be used explicitly. Instead, a perturbation method must be used to determine H_{eff} in the form of a perturbative series up to a certain order. To do so, we start by defining another operator $Q_0 = I - P_0$ in order to decompose the perturbation into a block-diagonal part $V_{\text{d}} = \mathscr{D}(V)$ and a block-off-diagonal part $V_{\text{od}} = \mathscr{O}(V)$ where $\mathscr{D}$ and $\mathscr{O}$ are superoperators:

$$\mathscr{D}(X) = P_0 X P_0 + Q_0 X Q_0$$

$$\mathscr{O}(X) = P_0 X Q_0 + Q_0 X P_0$$

We also, for an arbitrary operator Y, define the superoperator $\hat{Y}(X)$ as

$$\hat{Y}(X) = [Y, X]$$

Lastly, we introduce the superoperator $\mathscr{L}$, which applies the perturbation theory to the approach for finding H_{eff}:

$$\mathscr{L}(X) = \sum_{i,j} \frac{\langle i|\,\mathscr{O}(X)\,|j\rangle}{E_i - E_j} |i\rangle\langle j| \tag{2.19}$$

where $\{|i\rangle\}$ is an orthonormal eigenbasis of H_0. To derive the series, we begin by rewriting the transformed Hamiltonian $UHU^\dagger$ as

$$\exp(\hat{S})(H_0 + \eta V) = \cosh(\hat{S})(H_0 + \eta V_{\text{d}}) + \sinh(\hat{S})(H_0 + \eta V_{\text{od}}) + \cosh(\hat{S})(H_0 + \eta V_{\text{od}}) + \sinh(\hat{S})(H_0 + \eta V_{\text{d}}) \tag{2.20}$$

which, through posing the condition of the transformed Hamiltonian being block-diagonal and through some algebraic simplification [14], results in the expressions

$$\tanh(\hat{S})(H_0 + \eta V_{\text{d}}) + \eta V_{\text{od}} = 0 \tag{2.21}$$

$$\exp(\hat{S})(H_0 + \eta V) = H_0 + \eta V_{\text{d}} + \tanh(\hat{S}/2)(\eta V_{\text{od}}) \tag{2.22}$$

which will be used to determine S and H_{eff} respectively. Treating S as an infinitesimally small block-off-diagonal operator allows us to obtain

$$S = \mathscr{L}\hat{S}(\eta V_{\text{d}}) + \mathscr{L}\hat{S}\coth(\hat{S})(\eta V_{\text{od}}) \tag{2.23}$$

from Eq. 2.21. The infinitesimal condition also allows us to write S in a Taylor series form,

$$S = \sum_{n=1}^{\infty} S_n \eta^n \tag{2.24}$$

The S_n are finally given by

$$\begin{aligned} S_1 &= \mathscr{L}(V_{\text{od}}) \\ S_2 &= -\mathscr{L}\hat{V}_{\text{d}}(S_1) \\ S_n &= -\mathscr{L}\hat{V}_{\text{d}}(S_{n-1}) + \sum_{j\geq 1} a_{2j}\mathscr{L}\hat{S}^{2j}(V_{\text{od}})_{n-1} \end{aligned} \tag{2.25}$$

where the coefficient a arises from the Taylor series of $x\coth(x)$ (see Appendix A). In other words, Eq. 2.25 gives us an inductive formula that provides us with the Taylor coefficients S_n, which allows us to give an expression for the effective Hamiltonian. Similarly to the S operator, H_{eff} also partially consists of a Taylor series with coefficients $H_{\text{eff},n}$:

$$H_{\text{eff},n} = \sum_{j\geq 1} b_{2j-1} P_0 \hat{S}^{2j-1}(V_{\text{od}})_{n-1} P_0 \tag{2.26}$$

where cooefficients b arise from the Taylor expansion of the function $\tanh(x/2)$ (see Appendix A). Using P_0 to project Eq. 2.22 onto the low-energy subspace helps us obtain the final full form of the low-energy Hamiltonian:

$$H_{\text{eff}} = H_0 P_0 + \eta P_0 V P_0 + \sum_{n=2}^{\infty} \eta^n H_{\text{eff},n} \tag{2.27}$$

Worth noting is that an n^{th} order correction to H_{eff} only requires $n-1$ coefficients of S.

To summarize, we have established a method to simplify the Hamiltonian of a system by reducing it to an effective Hamiltonian acting only withing a desired low-energy subspace. By identifying the low-energy subspace in the form of projectors, a unitary transformation is applied consisting of series coefficients S_n which finally let us express the effective Hamiltonian H_{eff}.

2.4. Spin-Orbit Interaction In Germanium

Germanium (Ge) has emerged as a promising material for spin qubits and applications in the field of quantum computation and spintronics due to several advantageous properties. It has a low nuclear spin density thanks to the high abundance of isotopes with zero nuclear spin, which minimizes hyperfine interactions that typically cause decoherence. The relatively high atomic number of Germanium (32) causes the inner electrons to move at relativistic speeds, leading to stronger spin-orbit coupling than in other traditional semiconductor materials such as silicon. This allows for EDSR, meaning faster and more energy-efficient qubit operations through electrically controlled spins. Furthermore, high hole mobility and low effective mass speed up charge and spin transport, which is favorable for scaling up quantum dot arrays and improving qubit performance [15].

So far, we have handled simple SQD and DQD models to get an idea of the type of interactions that take place in the quantum dot system, and what calculations need to be made in order to find out the necessary parameters for controlling the spin qubit. In this section, we will explore the type of interactions expected in germanium structures by introducing the Luttinger-Kohn Hamiltonian, and we will show the steps that need to be taken to arrive at the Hamiltonian describing a DQD in a Ge bilayer.

2.4.1. The Luttinger-Kohn (LK) Hamiltonian

The Luttinger-Kohn Hamiltonian is a key theoretical model in the study of the electronic band in germanium and other semiconductor materials, especially for understanding hole behavior in the valence band. It was first introduced in the 1950s by J.M. Luttinger and W. Kohn [16], and provides a comprehensive description of interaction effects and effective mass in the valence band, typically comprising light holes, heavy holes and split-off bands. The Hamiltonian is founded on the framework of $\mathbf{k}\cdot\mathbf{p}$ perturbation theory, where the localized wave functions are expressed as superpositions of Bloch states at the Γ-point, i.e. at center of the Brillouin zone ($k=0$), and which encapsulates the symmetries of the crystal structure of the semiconductor material[17].

A common depiction of the Luttinger-Kohn Hamiltonian is in the form of a matrix in the basis of total hole angular momentum eigenstates $|j,m_j\rangle \in \{|\frac{3}{2},\frac{3}{2}\rangle,|\frac{3}{2},\frac{1}{2}\rangle,|\frac{3}{2},-\frac{1}{2}\rangle,|\frac{3}{2},-\frac{3}{2}\rangle,|\frac{1}{2},\frac{1}{2}\rangle,|\frac{1}{2},-\frac{1}{2}\rangle\}$:

$$H_{\mathrm{LK}} = \begin{bmatrix} P+Q & -S & R & 0 & -S/\sqrt{2} & \sqrt{2}R \\ -S^* & P-Q & 0 & R & -\sqrt{2}Q & \sqrt{3/2}S \\ R^* & 0 & P-Q & S & \sqrt{3/2}S^* & \sqrt{2}Q \\ 0 & R^* & S^* & P+Q & -\sqrt{2}R^* & -S^*/\sqrt{2} \\ -S^*/\sqrt{2} & -\sqrt{2}Q^* & \sqrt{3/2} & -\sqrt{2}R & P+\Delta & 0 \\ \sqrt{2}R^* & \sqrt{3/2}S^* & \sqrt{2}Q^* & -S/\sqrt{2} & 0 & P+\Delta \end{bmatrix} \tag{2.28}$$

All essential physics of the quantum dot is contained in the elements of this matrix:

$$\begin{aligned} P &= \frac{\hbar^2}{2m_0}\gamma_1(k_x^2+k_y^2+k_z^2) \\ R &= \sqrt{3}\frac{\hbar^2}{2m_0}[-\gamma_2(k_x^2-k_y^2)+2i\gamma_3 k_x k_y] \\ Q &= -\frac{\hbar^2}{2m_0}\gamma_2(k_z^2-k_x^2-k_y^2) \\ S &= \sqrt{3}\frac{\hbar^2}{m_0}(k_x-ik_y)k_z \end{aligned}$$

where m_0 denotes the free electron mass, γ_1,γ_2 and γ_3 are the so called Luttinger parameters which reflect symmetry properties of the bulk structure, and k_x, k_y and k_z are wave vectors capturing quantum confinement and band offsets. Finally, Δ represents the energy splitting between the highest valence bands and the split-off band at the Γ-point [15]. Another typical notation for the Hamiltonian is in the form of a spherical approximation:

$$H_{\mathrm{LK}} = -\frac{\hbar^2}{2m_0}\left[\left(\gamma_1+\frac{5}{2}\gamma_s\right)k^2-2\gamma_s(\mathbf{k}\cdot\mathbf{J})\right] \tag{2.29}$$

where $\hbar\mathbf{J}$ is the operator for effective spin 3/2. This form allows us to see that crystal momentum and effective spin are closely linked through the term $\mathbf{k}\cdot\mathbf{J}$, and that the Luttinger parameters relate to the mass leading to a grouping of the eigenstates of the Hamiltonian into states for heavy holes (HH) and states for light holes (LH)[18]. Due to strain that arises from the lattice mismatch due to differing lattice constants in quantum dots at the interfaces between materials, a correcting term should be added [19][20]:

$$H_{\text{strain}} = -E_s J_z^2 \tag{2.30}$$

where $E_s > 0$ is an additional strain energy. It turns out, though, that for low-energy states in germanium bilayers, the dimensionality of the Hamiltonian can be reduced, revealing spin-orbit interaction that is cubic in momentum.

2.4.2. Luttinger-Kohn for the germanium bilayer

In the case of 2D nanostructures such as the double quantum dot in a Ge bilayer that we are considering, it is advantageous to realize that the particle's movement is confined to the plane. In other words, one of the degrees of freedom is frozen meaning that the dimension of the Hamiltonian can be reduced. Furthermore, the LK Hamiltonians in Eq. 2.28 and Eq. 2.29 are specified in the basis of eigenstates of heavy holes and light holes, meaning that the required angular momentum (spin) operators are depicted as 4×4 matrices. The grouping of the eigenstates also results in dependence on the energy gap between the energetically lowest HH and LH states, commonly referred to as "HH-LH splitting $\Delta_{\text{HH-LH}}$". The 2D nature of the bilayer double dot structure leads to $\Delta_{\text{HH-LH}}$ becoming very large. As a consequence, we can approximate the system by ignoring the LH states when studying only the behavior of low-energy holes, and write the Hamiltonian via 2×2 Pauli matrices instead of 4×4 spin matrices[21].
In practice, the LK Hamiltonian undergoes a Schrieffer-Wolff transformation resulting in an expression that includes the effects of heavy holes and light holes on the ground state, and most importantly introduces spin-orbit interaction that is cubic in the in-plane momentum [22].

The Luttinger-Kohn Hamiltonian that the dimensional reduction gives, and that will be used for modeling the DQD in a germanium bilayer in Chap. 3 is finally given as (S.Bosco, private communication, May 2024):

$$H_{\text{LK}} = -\frac{\epsilon}{2}\tau_z + \frac{t}{2}\tau_x + \frac{p_+p_-}{2}\mathbf{m}\cdot\boldsymbol{\tau} - ip_+[p_+^2\boldsymbol{\alpha}_+\cdot\boldsymbol{\tau} - p_-^2\boldsymbol{\alpha}_-\cdot\boldsymbol{\tau}]\sigma_+ + \text{h.c.} - \frac{(p_+p_-)^2}{2}\mathbf{M}_+\cdot\boldsymbol{\tau} + \frac{(p_-^4+p_+^4)}{4}\mathbf{M}_-\cdot\boldsymbol{\tau} \tag{2.31}$$

We recognize the first two terms from the orbital Hamiltonian in Sec. 2.2.2, namely the detuning and tunneling contributions. Furthermore, 4-dimensional vectors are introduced that act on the layer degrees of freedom denoted $\boldsymbol{\tau} = (\tau_x, \tau_y, \tau_z, \tau_0)$, where τ_0 is the 2×2 identity. The vectors encapsulate material properties: $\mathbf{m}$ contains the effective masses in different directions and the components of $\boldsymbol{\alpha}_\pm$ are proportional to the Luttinger parameters $\gamma_2 \pm \gamma_3$. Similarly, the components of $\mathbf{M}_\pm \propto \gamma_2^2 \pm \gamma_3^2$, hence taking into account higher-order terms. Finally, $p_\pm = p_x \pm ip_y$ gives the in-plane momentum operators and $\sigma_\pm = \sigma_x \pm i\sigma_y$ the Pauli spin operators. H.c. is short for Hermitian conjugate.

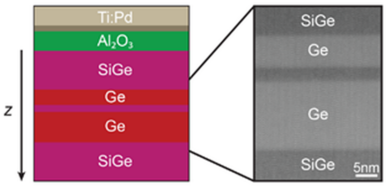

Figure 2.3: An example of a possible bilayer heterostructure. Two (asymmetric) quantum wells constructed in germanium and separated by SiGe. Figure taken from [23]

- Chapter 3 -

Results

3.1. Discretizing The Hamiltonian

The starting point of the calculation is to formulate a full Hamiltonian describing the system. We of course make use of the Hamiltonian in Eq. 2.31, but we must keep in mind that the spin-orbit interaction in the LK model can merely be considered as a perturbation of the energy levels determined by some potential. Since we are working with a quantum dot where the particles are confined in a well yet not restricted from tunneling, an appropriate choice is to model the confinement as a harmonic potential in the xy-plane:

$$V(x,y) = \frac{1}{2} m_0 \omega^2 (x^2 + y^2) \tag{3.1}$$

where we assume the confinement to be isotropic such that $\omega_x = \omega_y = \omega$. Furthermore, we want to add a term corresponding to a magnetic field $\mathbf{B}$ in the plane of the DQD. This takes the following form:

$$\begin{aligned} H_{\mathrm{m}} = g_0(B_+\sigma_- + B_-\sigma_+) + (B_+\sigma_- + B_-\sigma_+)(p_+p_-)\mathbf{g}_1 \cdot \boldsymbol{\tau} \\ + (B_+\sigma_+ + B_-\sigma_-)(p_+^2 + p_-^2)\mathbf{g}_{2,+} \cdot \boldsymbol{\tau} + (B_+\sigma_+ + B_-\sigma_-)(p_+^2 - p_-^2)\mathbf{g}_{2,-} \cdot \boldsymbol{\tau} \end{aligned} \tag{3.2}$$

where g_0 and the g-vectors represent the different in-plane Landé g-factors and $B_\pm = B_x \pm iB_y$. Worth noting is that momentum p and crystal momentum (wave vector) k are being used interchangeably because we for convenience have chosen $\hbar = 1$.

Since we have chosen a harmonic confinement potential, we will use the eigenfunctions of the harmonic potential to discretize the full Hamiltonian. They are given by:

$$\psi_{n_x}(x) = \frac{e^{-\frac{x^2}{2l_x^2}}}{\sqrt{l_x 2^n n! \sqrt{\pi}}} H_n\left(\frac{x}{l_x}\right) \tag{3.3}$$

in the x-direction and

$$\phi_{n_y}(y) = \frac{e^{-\frac{y^2}{2l_y^2}}}{\sqrt{l_y 2^n n! \sqrt{\pi}}} H_n\left(\frac{y}{l_y}\right) \tag{3.4}$$

in the y-direction, with the product of the two being the total eigenfunction of the potential. The functions H_n denote the Hermite polynomials, and $l_x = l_y = l = \sqrt{\hbar/m_0\omega}$ are the confinement lengths. We use these eigenfunctions to construct all the matrix components related to position and momentum, i.e. the potential term, the spin-orbit term, and the kinetic energy term, by simply calculating $\langle\psi_i|H|\psi_j\rangle$ and $\langle\phi_i|H|\phi_j\rangle$ for $i,j = 0,...,n$. For simplicity, the quartic momentum term in H_{LK} is omitted, as the quartic contribution, similarly to higher order terms in a series expansion, is small. To incorporate sufficiently significant interaction orders, the 6 lowest energy wavefunctions were used, i.e. the position and momentum contributions were computed up until $n = 6$ resulting in 6×6 matrices.
Before we can write down the whole Hamiltonian in matrix form, we have to pick an ordered basis so that we can systematically include different components using a tensor product. For this calculation, the ordered basis $|\text{spin}, \text{layer}, x, y\rangle$ was chosen. This means that first spin-related σ terms are added up, layer-related τ terms are added up, x-position and x-momentum terms are added up etc., and that they are all combined through the tensor (Kronecker) product:

$$|\text{spin}\rangle \otimes |\text{layer}\rangle \otimes |n_x\rangle \otimes |n_y\rangle$$

The spin and layer both correspond to a 2×2 Hilbert space, whereas $|n_x\rangle$ and $|n_y\rangle$ reside in a 6×6 Hilbert space. As a result, the tensor product finally gives a full discretized Hamiltonian in the form of a 144×144 matrix.

3.2. g-factor And Exchange Anisotropy In Germanium Bilayer DQD

Getting any insight from such a big matrix is difficult. An appropriate next step to take is to make use of the Schrieffer-Wolff transform, in order to give the discretized Hamiltonian a more familiar form. First, the projector P_0 is found by identifying the positions of the ground state on the diagonal of the matrix. Second, an order of perturbation is chosen up to which the effective Hamiltonian is calculated. For our purposes, a second-order Schrieffer-Wolff is sufficient to portray the interactions that we are interested in.
The transformation helps us land in a 4×4 matrix in an equivalent singlet-triplet basis as introduced in Sec.2.2.4, which can be split up into the first-order correction H_1 (see Appendix A) and the second-order correction H_2. To view the results, we use provided numerical data for a symmetric (unlike the asymmetric structure shown in Fig. 2.3) double quantum dot of well width 15nm and interdot distance 3nm in a germanium bilayer (S. Bosco, private comm. June 2024). The spin-orbit effects are finally demonstrated through the calculation of g-factor anisotropy in x- and z-direction. The difference in g-factors between the dots, δg_x and δg_z, is plotted against the dot size l for three different cases: zero detuning ($\epsilon = 0$), small detuning ($\epsilon = 0.18$meV) and large detuning ($\epsilon = 1.8$meV).

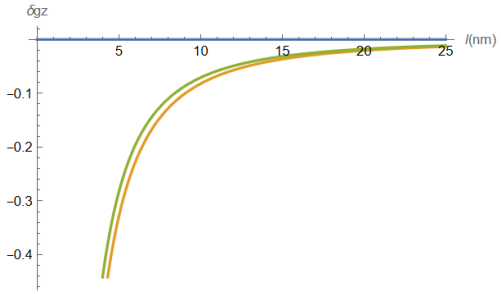

(a) First-order δg_z correction

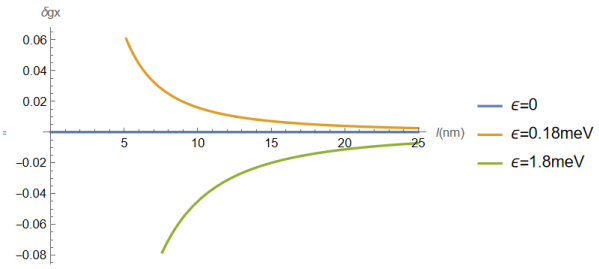

(b) First-order δg_x correction

Figure 3.1: The first order correction on the quantum system. The g-factor difference scales with $\pm l^{-2}$ when detuning is present, whereas δg remains constant at zero when $\epsilon = 0$. The magnetic field is applied in the xy-plane.

In Fig. 3.1, we see that δg is inversely proportional to the dot size squared for the cases with detuning, and constant at zero without detuning. The $\epsilon = 0$ case makes sense since we are dealing with a perfectly symmetrical dot where the energies are the same. As the detuning is increased, the symmetry between the top and the bottom layer is broken, and the sign tells us which dot has the larger g-factor.

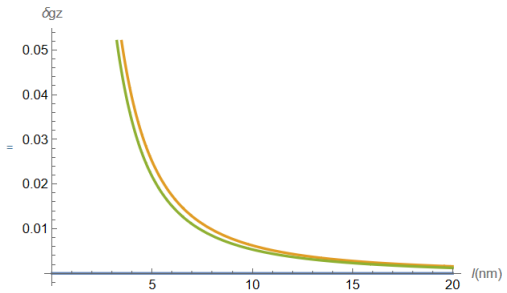

(a) Second-order δg_z correction

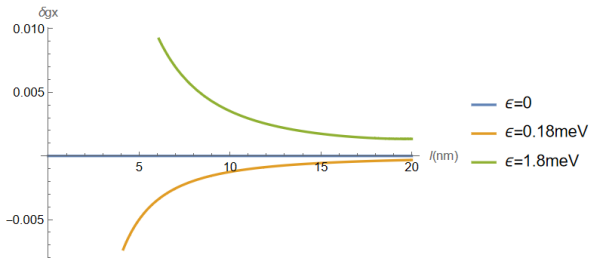

(b) Second-order δg_x correction

Figure 3.2: The second-order correction on the quantum system. The g-factor difference still scales with $\pm l^{-2}$ with detuning is present. Note that signs are flipped and that the corrections are roughly an order of magnitude smaller than in the first order.

Fig. 3.2 shows the second-order correction, and we deduce that δg, as expected, is still constant at zero with no detuning present. Furthermore, the change of sign indicates that the second-order correction favors the opposite dot compared to the first order. Worth noting is also that the corrections shown in the second plot are roughly one order of magnitude smaller than in the first one.
The relationship between δg and l seems to be inversely squared in the second-order correction too, but something interesting happens when we start considering larger dot sizes, as demonstrated in Fig 3.3.

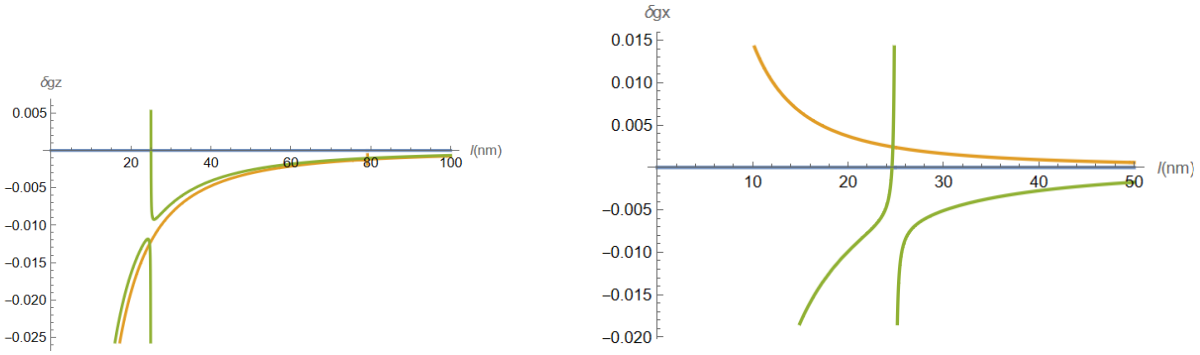

(a) Total δg_z correction

(b) Total δg_x correction

Figure 3.3: When we consider larger dot sizes, divergences show up in the plots at an l-value of 79nm for $\epsilon = 0.18$meV and at $l = 26nm$ for $\epsilon = 1.8$meV.

The divergences that show up can be explained by a critical dot size; as the dots become larger and larger, the orbital gap reduces until a point where it is smaller than the energy splitting due to detuning and tunneling, $\sqrt{\epsilon^2 + t^2}$. By recalling that the Schrieffer-Wolff transformation, which was used to obtain these results, relies on a sufficiently large energy gap between the low-energy subsector and the rest of the states, we can conclude that the transformation loses its validity for dot sizes larger than the critical l-value due to the appearance of an additional energy state. The critical value is related to the detuning and the tunnel coupling by $1/l^2 \propto \sqrt{\epsilon^2 + t^2}$, explaining why the larger detuning case sees the divergence at a lower value of l.

Finally, we also compute and plot the rotation angle ϑ of the exchange due to g-factor anisotropy through the use of the expression found in Sec.2.2.4, Eq. 2.16:

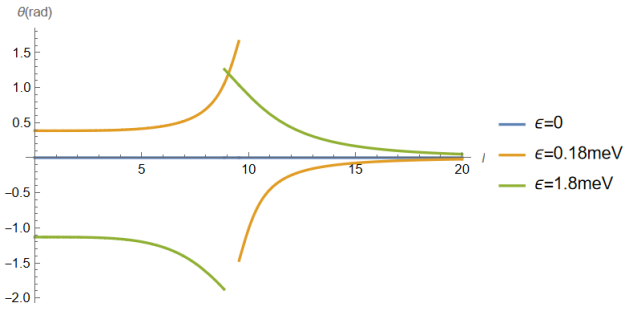

Figure 3.4: Angle of rotation of the exchange associated with an anisotropic Zeeman field.

In the figure, we see how the rotation angle depends on the size of the dot. Once again, the $\epsilon = 0$ case yields no rotation. The discontinuities that show up for the detuned cases have a gap of π, suggesting a flip of the angle at certain values of l ($l = 9.55$nm for $\epsilon = 0.18$meV and $l = 8.88$nm for $\epsilon = 1.8$meV). However, the main explanation for the jumps is most likely simply the range of the $\arctan(x)$ function. The value of the rotation angle as l goes to zero converges to 0.38 radians for $\epsilon = 0.18$meV and to -1.13 radians for $\epsilon = 1.8$meV.

- Chapter 4 -

Conclusion and Outlook

In summary, this project aimed to theoretically model a double quantum dot in a germanium bilayer to identify and explore the effects caused by spin-orbit interactions. This was done by discretizing the Luttinger-Kohn Hamiltonian in a harmonic potential and finding an effective energy description by projecting the Hamiltonian onto a low-energy subspace using the Schrieffer-Wolff transformation. The spin-orbit interaction effects are analyzed by comparing anisotropy in the Landé g-factor with the size of the quantum dots in the layers.
The results suggest that symmetrical dots in a germanium bilayer without any detuning experience no difference in g-factor. When detuning is present the dot size l is limited due to a reduction in the energy gap between upper- and lower-layer orbitals causing the Schrieffer-Wolff transformation to break down and extra energy levels to be added to the effective system.
Comparing this model with monolayer DQD structures would be a next step in this research to help get a better understanding of the effects that two interacting spins have on each other. This would ultimately lead to more accurate modelling and construction of two-qubit gates, setting a milestone in the field of germanium use for quantum computing.

- Chapter 5 -

Acknowledgments

I would like to express my sincerest gratitude to my supervisor Stefano Bosco for his guidance and support throughout the project. Special thanks also goes out to the QCD theory group at QuTech for the interesting discussions and meetings.

Bibliography

[1] G. Burkard, T. D. Ladd, A. Pan, J. M. Nichol, and J. R. Petta, "Semiconductor spin qubits," *Reviews of Modern Physics*, vol. 95, June 2023.

[2] J. M. Elzerman, R. Hanson, L. H. Willems van Beveren, B. Witkamp, L. M. K. Vandersypen, and L. P. Kouwenhoven, "Single-shot read-out of an individual electron spin in a quantum dot," *Nature*, vol. 430, p. 431–435, July 2004.

[3] D. Loss and D. P. DiVincenzo, "Quantum computation with quantum dots," *Physical Review A*, vol. 57, p. 120–126, Jan. 1998.

[4] J. R. Petta, A. C. Johnson, J. M. Taylor, E. A. Laird, A. Yacoby, M. D. Lukin, C. M. Marcus, M. P. Hanson, and A. C. Gossard, "Coherent manipulation of coupled electron spins in semiconductor quantum dots," *Science*, vol. 309, no. 5744, pp. 2180–2184, 2005.

[5] W. I. L. Lawrie, H. G. J. Eenink, N. W. Hendrickx, J. M. Boter, L. Petit, S. V. Amitonov, M. Lodari, B. Paquelet Wuetz, C. Volk, S. G. J. Philips, G. Droulers, N. Kalhor, F. van Riggelen, D. Brousse, A. Sammak, L. M. K. Vandersypen, G. Scappucci, and M. Veldhorst, "Quantum dot arrays in silicon and germanium," *Applied Physics Letters*, vol. 116, Feb. 2020.

[6] S. P. Harvey, "Quantum dots/spin qubits," Feb. 2022.

[7] L. C. Camenzind, S. Geyer, A. Fuhrer, R. J. Warburton, D. M. Zumbühl, and A. V. Kuhlmann, "A hole spin qubit in a fin field-effect transistor above 4kelvin," *Nature Electronics*, vol. 5, p. 178–183, Mar. 2022.

[8] "Intel and qutech demonstrate high-fidelity 'hot' qubits for practical quantum systems," Apr. 2020.

[9] Y. A. Bychkov and E. I. Rashba, "Oscillatory effects and the magnetic susceptibility of carriers in inversion layers," *Journal of Physics C: Solid State Physics*, vol. 17, p. 6039, nov 1984.

[10] S. Nadj-Perge, S. M. Frolov, E. P. A. M. Bakkers, and L. P. Kouwenhoven, "Spin–orbit qubit in a semiconductor nanowire," *Nature*, vol. 468, p. 1084–1087, Dec. 2010.

[11] W. A. Coish and D. Loss, "Quantum computing with spins in solids," 2006.

[12] D. P. Arovas, E. Berg, S. A. Kivelson, and S. Raghu, "The hubbard model," *Annual Review of Condensed Matter Physics*, vol. 13, p. 239–274, Mar. 2022.

[13] S. Geyer, B. Hetényi, S. Bosco, L. C. Camenzind, R. S. Eggli, A. Fuhrer, D. Loss, R. J. Warburton, D. M. Zumbühl, and A. V. Kuhlmann, "Two-qubit logic with anisotropic exchange in a fin field-effect transistor," 2022.

[14] S. Bravyi, E.-m. d.-j. DiVincenzo, David P., and D. Loss, "Schrieffer-wolff transformation for quantum many-body systems," *Annals of Physics (New York)*, vol. 326, 10 2011.

[15] L. A. Terrazos, E. Marcellina, Z. Wang, S. N. Coppersmith, M. Friesen, A. R. Hamilton, X. Hu, B. Koiller, A. L. Saraiva, D. Culcer, and R. B. Capaz, "Theory of hole-spin qubits in strained germanium quantum dots," *Physical Review B*, vol. 103, Mar. 2021.

[16] J. M. Luttinger and W. Kohn, "Motion of electrons and holes in perturbed periodic fields," *Phys. Rev.*, vol. 97, pp. 869–883, Feb 1955.

[17] J. M. Luttinger, "Quantum theory of cyclotron resonance in semiconductors: General theory," *Phys. Rev.*, vol. 102, pp. 1030–1041, May 1956.

[18] G. Scappucci, C. Kloeffel, F. A. Zwanenburg, D. Loss, M. Myronov, J.-J. Zhang, S. De Franceschi, G. Katsaros, and M. Veldhorst, "The germanium quantum information route," *Nature Reviews Materials*, vol. 6, p. 926–943, Dec. 2020.

[19] G. L. Bir and G. E. Pikus, "Symmetry and strain-induced effects in semiconductors," 1974.

[20] M. Luethi, K. Laubscher, S. Bosco, D. Loss, and J. Klinovaja, "Planar josephson junctions in germanium: Effect of cubic spin-orbit interaction," *Physical Review B*, vol. 107, Jan. 2023.

[21] R. Winkler, D. Culcer, S. J. Papadakis, B. Habib, and M. Shayegan, "Spin orientation of holes in quantum wells," *Semiconductor Science and Technology*, vol. 23, p. 114017, Oct. 2008.

[22] D. V. Bulaev and D. Loss, "Electric dipole spin resonance for heavy holes in quantum dots," *Phys. Rev. Lett.*, vol. 98, p. 097202, Feb 2007.

[23] A. Tosato, B. M. Ferrari, A. Sammak, A. R. Hamilton, M. Veldhorst, M. Virgilio, and G. Scappucci, "A high-mobility hole bilayer in a germanium double quantum well," 2022.

- Appendix A -

Coefficients and Matrices

A.1. Taylor series coefficients

Taylor series of $x\coth(x)$:

$$x\coth(x) = \sum_{n=0}^{\infty} a_{2n} x^{2n}, \quad a_m = \frac{2^m B_m}{m!} \tag{A.1}$$

Taylor series of $\tanh(x/2)$:

$$\tanh(x/2) = \sum_{n=0}^{\infty} b_{2n-1} x^{2n-1}, \quad b_{2n-1} = \frac{2(2^{2n} - 1 B_{2n}}{(2n)!} \tag{A.2}$$

with B_m the Bernoulli numbers.

A.2. Effective Hamiltonian H1

$$\begin{bmatrix} \frac{2m_0+m_z-l^2\epsilon}{2l^2} & \frac{1}{2}(\frac{m_x}{l^2}+t) & \frac{2B_-(g_{1,0}+g_{1,z}+g_0 l^2)}{l^2} & \frac{2B_- g_{1,x}}{l^2} \\ \frac{1}{2}(\frac{m_x}{l^2}+t) & \frac{2m_0-m_z+l^2\epsilon}{2l^2} & \frac{2B_- g_{1,x}}{l^2} & \frac{2B_-(g_{1,0}-g_{1,z}+g_0 l^2)}{l^2} \\ \frac{2B_+(g_{1,0}+g_{1,z}+g_0 l^2)}{l^2} & \frac{2B_+ g_{1,x}}{l^2} & \frac{2m_0+m_z-l^2\epsilon}{2l^2} & \frac{1}{2}(\frac{m_x}{l^2}+t) \\ \frac{2B_+ g_{1,x}}{l^2} & \frac{2B_+(g_{1,0}-g_{1,z}+g_0 l^2)}{l^2} & \frac{1}{2}(\frac{m_x}{l^2}+t) & \frac{2m_0-m_z+l^2\epsilon}{2l^2} \end{bmatrix} \tag{A.3}$$